minerals

MDPI

Article

Different Insights into Silicate Rectorite Modification and Its Role in Removal of Heavy Metal Ions from Wastewater

Ya Gao, Hao Jiang *, Xianyuan Li, Sultan Ahmed Khoso, Guoyuan Xiang and Wenping Han

School of Minerals Processing and Bioengineering, Central South University, Changsha 410083, China; gaoyacsu@126.com (Y.G.); dyyslxy861490@163.com (X.L.); sultan.khoso@faculty.muet.edu.pk (S.A.K.); xiangguoyuan@126.com (G.X.); hanwenping9305@163.com (W.H.)

* Correspondence: jianghao-1@126.com; Tel.: +86-731-8883-0545

Received: 17 December 2019; Accepted: 11 February 2020; Published: 15 February 2020

Abstract: In the field of water management, the separation of metal contaminants from wastewater is very important and challenging. This study systematically investigated the effect and underlying mechanism of silicate rectorite (REC) on the removal of heavy metal ions (Cr(VI) and Pb(II)) from wastewater. The adsorption and removal capacity of REC was further improved by its novel modification with ferric chloride hexahydrate. Compared to natural REC, the modified rectorite (Fe-REC) showed comparatively superior adsorption efficiency for both Cr(VI) and Pb(II) due to the chemisorption of Fe^{3+} on the REC surface as its oxidation state (Fe–O, Fe–OH, Fe–OOH). Adsorption on Cr(VI) attributed to the reaction between iron hydroxy complexes ($FeOH^{2+}$, $Fe(OH)_2{}^{+}$ and $Fe(OH)_3$(aq)) and Cr(VI) species ($HCrO_4{}^{-}$ and $CrO_4{}^{2-}$) in the aqueous solution. This reaction was perfectly consistent with the binding energy shifts in O 1s and Fe 2p species, as reflected by XPS analysis. While, the existence of –Al–OH and –Si–OH in silicate REC slurry reacted with $PbOH^{+}$ colloids produced from lead ions hydrolysis to promote Pb(II) adsorption. Zeta potential after modification and removal occurred to shift positively or negatively to testify the adsorption of Fe^{3+} and heavy metal ions. Freundlich and Langmuir isotherms conformed adsorption process for Cr(VI) and Pb(II), respectively.

Keywords: rectorite; ferric chloride hexahydrate; modification; adsorption; heavy metal ions

1. Introduction

A long-standing problem, heavy metal ions contaminations from wastewater, is being in dire need of a solution to be solved thoroughly due to their biological accumulation and higher toxicity even at minute concentrations. Generally, the majority of these pollutants cannot degrade by themselves, such as hexavalent chromium Cr(VI) and divalent lead Pb(II). Hexavalent chromium is a kind of strong oxidant and highly soluble heavy metal with carcinogenic, mutagenic and teratogenic substance for human [1,2]. Based on its long-term impact, Cr(VI) has been listed as the first-class A toxic pollutant by the U.S. Environmental Protection Agency [3]. While Pb(II) acts as one of the most harmful heavy metals [4], plumbism by accumulation in human body can result in damages in brain, nervous, metabolic and reproductive system, even trigger sickness or death [5,6]. The bulk of these contaminations as effluents are discharged from several industries, including mining, batteries, textiles, metal plating, etc. [7].

Currently, more and more techniques have been developed and utilized for the removal of heavy metals from the aqueous environments, such as adsorption, electrochemistry, precipitation reaction, membrane filtration and biosorption processes [8,9]. Among these, the adsorption is an effective

and economical approach that is widely used in wastewater treatment procedures. In adsorption, a variety of adsorbent including activated carbons, clay mineral, biomasses and synthetic polymers was employed [8,10–13]. However, common adsorbents such as activated carbon are expensive, thus some natural resources such as polysaccharides, fly ash and clay have attracted much attention due to their low cost and easy access. In this series of materials, rectorite (REC) was applied more and more in pollutant adsorption from sewage owing to its low cost, high ion exchange capacity and relatively large specific area [14–17]. It is a sort of rare regularly interstratified silicate and similar to kaolinite. Its special structure is alternate pairs of dioctahedral mica-like layer (non-expansible) and dioctahedral smectite-like layer (expansible) existing in 1:1 ratio. There are some cations (Na^+, K^+ and Ca^{2+}) and hydrated cations with exchangeability, which can enlarge its interlayer distance by intercalating cations or polar molecules existing in the interlayer regions.

Over several decades, there are more and more investigations on the adsorption of metal ions by REC or its synthesis [17–21]. For example, Mei et al. [17] and Zhao et al. [22] studied separately the adsorption behaviors of Pb(II) by Ca-rectorite and Sr(II) by Na-rectorite as a function of different environmental parameters including the influence of pH, temperature, ionic strength and humic acid (HA) under ambient conditions. Both of them found that the adsorption results of heavy metals were intensely decided by pH and ionic strength and the adsorption process was spontaneous and endothermic. In addition, more and more synthetic composite materials of REC have been researched to adsorb different pollutants [18–20,23]. These composites can combine both excellent performances of their components, such as good thermostability, mechanical property and adsorption capacity, the synergies can help them obtain superior adsorption capacity to heavy metal ions [24]. However, many existing studies just concentrated on the feasibility of adsorption of REC on different kinds of harmful pollutants, while its adsorption mechanism, especially how the adsorption process happens, still remains to make them understood thoroughly.

In this paper, the adsorption performance of REC on heavy metal ions was studied including hexavalent chromium ions (Cr(VI)) and divalent lead ions (Pb(II)) and then uncovered its underlying mechanism. In order to make it more exchangeable and improve its adsorption capacity, REC was further modified with addition of ferric chloride (Fe-REC), which was never employed in the modification of rectorite to obtain activation effects and weaken the interlayer bond force of REC. Afterwards, the surface potential and XPS analyses were employed to explain the adsorption behaviors of ions on the REC surface. Simultaneously, the species distribution in rectorite slurry and adsorption isotherms was calculated respectively to reflect its adsorption mechanism. We believe that the results would be of significance to the mechanism of rectorite modification and adsorption research and heavy metal ion wastewater treatment.

2. Materials and Methods

2.1. Samples and Chemicals

The object of present investigation, rectorite, was received from Zhongxiang City, Hubei Province, China. After a series of physical upgrading processes, including manual crushing, hand-picking, porcelain milling and dry screening, this monomineral samples of rectorite were stored in the jar for subsequent researches. The chemical composition (XRF) and X-ray diffractometry (XRD) were carried out to examine the purity of rectorite samples (−0.074 mm). XRF (Panalytical.B.V, Almelo, The Netherlands) was measured by the method of "Omnia+5", while the voltage and vacuum degree were controlled at 60 kV and 2 Pa. For XRD (Bruker, Karlsruhe, Germany), its test minimum step was 0.0001°, the voltage and current were less than 40 kV and 40 mA, respectively. Table 1 showed that the main compositions of the sample were Al_2O_3 and SiO_2 respectively, which were exactly the theoretical compounds of rectorite. According to Figure 1, the XRD peaks of rectorite were very obvious. There, the results shown in Table 1 and Figure 1 revealed that the purity of samples was approximately 90%, which was qualified enough to be used in analytical measurements.

Table 1. Chemical composition of mineral sample (mass fraction, %).

Sample	Al_2O_3	SiO_2	Fe_2O_3	TiO_2	CaO	MgO	K_2O	Na_2O	LOI [1]
Rectorite	36.53	47.41	0.4	4.34	5.44	0.31	0.71	1.23	3.94

"1" Loss on ignition.

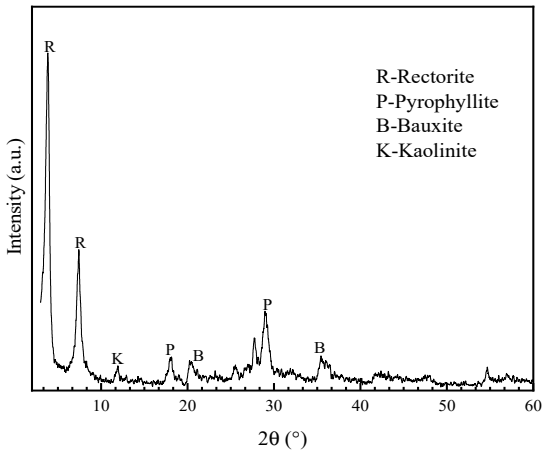

Figure 1. XRD pattern of the purified rectorite.

Ferric chloride hexahydrate ($FeCl_3 \cdot 6H_2O$) was used for the modification of rectorite. Potassium dichromate ($K_2Cr_2O_7$) and lead nitrate ($Pb(NO_3)_2$) of chemical purity were used as simulated wastewater sources of the pollution respectively. In addition, HCl and NaOH of analytical grade from Damao Chemical Reagent Factory China (Tianjin, China) were used to control the pH through glass dropper bottles to eliminate the influence of the volume change of slurry. Different drops of HCl (3%, volume concentration) or NaOH (5%, mass concentration) were added to control the pH to the desired value. Ultrapure water was used throughout the study.

2.2. Methods

2.2.1. Rectorite Modification

Rectorite modification was conducted in a constant temperature oscillator with leaching as the main method. A certain amount of rectorite sample was added in the freshly prepared modifier Fe^{3+} solution with a certain concentration, followed by the agitation with a constant temperature oscillator of 180 r/min speed under 30 °C. The modified rectorite sample (Fe-REC) was collected by the centrifugation, then washed several times with de-ionized water to remove the residual modifier and dried in a vacuum oven at 85 °C for 6 h.

2.2.2. Heavy Metal Ions Adsorption Test

The residual metal concentration of rectorite pulp after the adsorption process was determined by inductively coupled plasma spectrometer (ICP; Spectro, Kleve, Germany). During the measurements, the temperature was kept at 25 °C. The samples used in this adsorption test were prepared in the following order: at first, the modified sample Fe-REC was mixed simulated wastewater of 30 mg/L Cr(VI) and 40 mg/L Pb(II), respectively. Two kinds of mixtures were then shaken in the constant temperature oscillator for a while (10–70 min) to make the heavy metal ions adsorbed by Fe-REC efficiently. In the subsequent step, the liquid fraction that separated from the slurry was analyzed for the adsorption measurements. The procedure of modification and adsorption is provided in Figure 2.

At last, the adsorbed amounts (represented by Γ) of Cr(VI) and Pb(II) by modified rectorite surface were calculated by using following equation:

$$\Gamma = \frac{C_0 - C}{C_0} \times 100\% \quad (1)$$

where Γ is the adsorbed amount of heavy metal ions; C_0 and C are the initial and residual concentrations (mg/L), respectively;

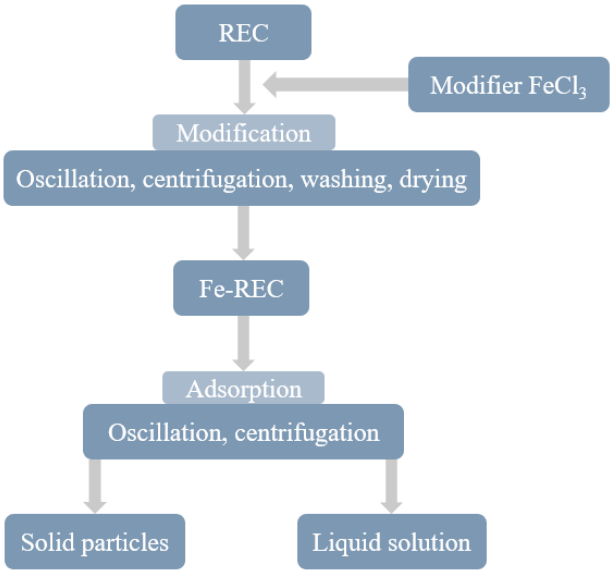

Figure 2. Schematic diagram of the procedure of modification and adsorption.

2.2.3. Zeta Potential Test

Zeta potential measurements were conducted by a Coulter Delsa 440sx Zeta potential analyzer (Beckman Coulter, Beea, CA, USA) equipped with a rectangular electrophoresis cell. For the measurements, mineral samples were ground to –2 μm and the suspension was prepared by adding 40 mg of mineral samples to 80 mL desired solutions containing 1 mmol/L KNO_3 as supporting electrolytes. Then, the suspension was conditioned by a magnetic stirring for 6 min to ensure adequate dispersion of the fine mineral particles. After settling for 10 min, the supernatant of the dilute fine particle suspension was taken for the zeta potential measurements.

2.2.4. XPS Analysis

X-ray Photoelectron Spectroscopy (XPS) with K-Alpha$^+$ (Thermo fisher Scientific, Waltham, MA, USA) was applied to analyze the composition and chemical state of the elements on the mineral surface before and after its modification and adsorption in order to characterize if the modifier Fe^{3+} and the heavy metal ions Cr(VI) and Pb(II) were adsorbed effectively. The vacuum in the analysis room was kept at about 2×10^{-7} mba and the X-ray source was monochromatic Al Ka at the energy of 72 W with 400 μm. Additionally, the scanning mode was decided as CAE. The energy step size of survey spectra and high-resolution spectra were 1.00 eV and 0.1 eV, respectively and their pass energy was set at 100 eV and 30 eV, respectively. All binding energies were calibrated using a characteristic C1s carbon peak (C1s = 284.7 eV). The sample was filtered and washed repeatedly with ultrapure water for washing away the weak physical adhesion of the reagent on the mineral surface. Afterwards, it was dried in a vacuum oven and then used for testing.

2.2.5. Description of Solution Chemistry Calculations

It is rather necessary to comprehend the occurrence state and physicochemical behavior of metal ions in the slurry. The adsorption of modifier Fe^{3+} and heavy metal ions Cr(VI) and Pb(II) on the rectorite surface related to their dissolved state and hydrolyzed components to a degree. As a result, the solution compositions of Fe^{3+}, Cr(VI) and Pb(II) were calculated to understand the mechanism of modification and adsorption. Metal ions can be hydrolyzed in the aqueous solution to form different hydroxy complexes. At this time, the concentration of each component can be calculated from the equilibrium relationship in the aqueous solution.

The species distribution of Fe^{3+} in solutions was influenced by its pH and the initial concentration simultaneously. Homogeneous and heterogeneous systems were named before and after the precipitation reactions occurred, which were affected by the pH of solution. Different systems had different computing methods. In homogeneous ferric chloride solution system, the equilibrium reaction formulas and corresponding reaction coefficient were as follows [25]:

The initial concentration of Fe^{3+} and its side reaction coefficients were recorded as C_{Fe} and $\alpha_{Fe^{3+}}$, respectively, then:

$$\alpha_{Fe^{3+}} = 1 + \beta_1[OH^-] + \beta_2[OH^-]^2 + \beta_3[OH^-]^3 + \beta_4[OH^-]^4 \quad (2)$$

Subsequently, the species distribution of each component in homogeneous system was:

$$\left[Fe^{3+}\right] = C_{Fe}/\alpha_{Fe^{3+}} \quad (3)$$

$$\left[FeOH^{2+}\right] = \beta_1\left[Fe^{3+}\right][OH^-] \quad (4)$$

$$\left[Fe(OH)_2^+\right] = \beta_2\left[Fe^{3+}\right][OH^-]^2 \quad (5)$$

$$\left[Fe(OH)_{3(aq)}\right] = \beta_3\left[Fe^{3+}\right][OH^-]^3 \quad (6)$$

$$\left[Fe(OH)_4^-\right] = \beta_4\left[Fe^{3+}\right][OH^-]^4 \quad (7)$$

In heterogeneous system, the species distribution of each component was:

$$\left[Fe^{3+}\right] = K_{s0}/[OH^-]^3 \quad (8)$$

$$\left[FeOH^{2+}\right] = K_{s1}/[OH^-]^2 \quad (9)$$

$$\left[Fe(OH)_2^+\right] = K_{s2}/[OH^-] \quad (10)$$

$$\left[Fe(OH)_{3(aq)}\right] = K_{s3} \quad (11)$$

$$\left[Fe(OH)_4^-\right] = K_{s4}[OH^-] \quad (12)$$

$$\left[Fe(OH)_{3(s)}\right] = C_{Fe} - \left[Fe^{3+}\right] - \left[FeOH^{2+}\right] - \left[Fe(OH)_2^+\right] - \left[Fe(OH)_{3(aq)}\right] - \left[Fe(OH)_4^-\right] \quad (13)$$

3. Results and Discussion

3.1. Modification of Rectorite

Different influencing factors were studied in Figure 3 to obtain the Fe-REC smoothly, such as the time of modification and the concentrations of Fe^{3+} ions and pulp. Modification results were evaluated by the ability of modified rectorite to adsorb Cr(VI) ion in the solutions. As shown in Figure 3a, Fe^{3+} concentration had important effects on the adsorption rate of Cr(VI). The Cr(VI) adsorption rate increased rapidly with the increasing Fe^{3+} concentration up to 0.1 mol/L and then tended towards equilibrium with a further increase in doses of Fe^{3+}. The optimum adsorption rate (about 89%) was

obtained at the 0.1 mol/L Fe^{3+} concentration. When it comes to the effect of pulp concentration in Figure 3b, the Cr(VI) adsorption rate increased slowly when the pulp concentration ranged from 50 to 300 g/L. As can be noted, there was a minor decrease in the Cr(VI) adsorption rate by increasing the pulp concentration from 200 to 300 g/L. Namely, the higher the pulp concentration, the slower the growth rate. Consequently, 200 g/L was defined as optimal pulp concentration value for REC modification. If REC was modified for a longer time (shown in Figure 3c), less and less Cr(VI) ions were adsorbed on the REC surface making the adsorption rate deteriorated evidently. Affected by modified time, the highest adsorption rate of 88.94% appeared at 3 h, which would be utilized as the fabrication time of Fe-REC. Overall, different factors had different effects on the modification results with the following sequence: Fe^{3+} concentration > pulp concentration > modification time. In other words, the concentration of Fe^{3+} had the greatest impact on the modification results while the modified time was the minimum.

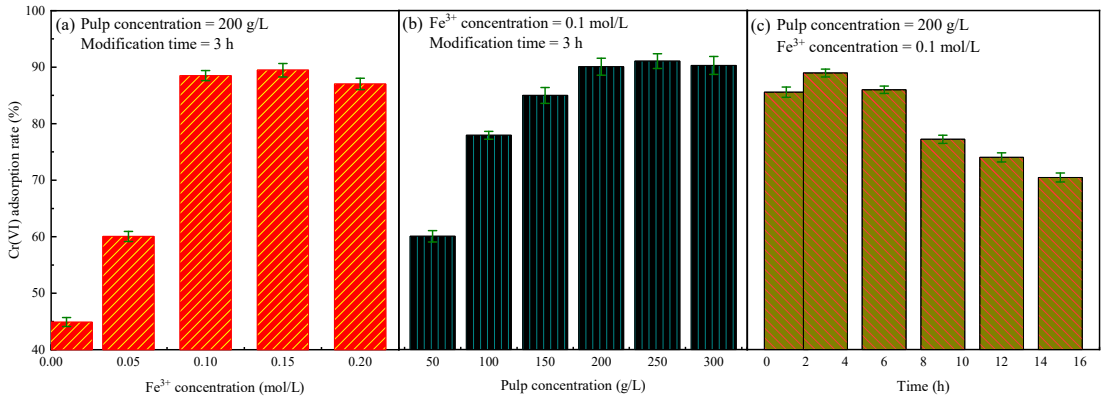

Figure 3. The modification effects of rectorite under three different factors. (**a**) Fe^{3+} concentration; (**b**) pulp concentration and (**c**) modification time.

3.2. Adsorption Studies

After the successful modification and obtaining Fe-REC, its adsorption performance on Cr(VI) and Pb(II) were investigated in the Figure 4 systematically. Figure 4a reflected the effect of pH on Cr(VI) and Pb(II) adsorption with REC and Fe-REC, respectively. As can be seen, the adsorption ability of Fe-REC was much better than that of the natural REC for both Cr(VI) and Pb(II), indicating that the Fe^{3+} modification greatly contributed to its adsorption capacity. For Cr(VI) ions, the adsorption rate with Fe-REC declined significantly from acidic environment to basic, while there was almost no fluctuation with natural REC where the adsorption rate stabled at 55% approximately. If the mineral was modified by Fe^{3+}, the natural pH of slurry was kept at 5 where the adsorption rate had approached 90%. Even though the pH of slurry was adjusted extremely acidic, the disparity to its natural pH was negligible. Hence there is no need to adjust the pulp pH for the sake of simplified experimental procedure. Compared with the Cr(VI) adsorption, there was an obvious difference in acidic and basic pulp for Pb(II) adsorption, in which the adsorption rate in basic pH was rather higher than that of the acidic no matter REC or Fe-REC. The main reason for this result was that in the presence of OH^-, Pb(II) ions would react with OH^- to form $Pb(OH)_2$ precipitate making it no significance for Pb(II) adsorption under alkaline environment. Like Cr(VI) adsorption, the optimum pH for Pb(II) adsorption was also fixed at its natural value.

Figure 4 showed the effect of pulp concentration on the adsorption of Cr(VI) and Pb(II). Similar to Figure 4a, there was an evident phenomenon that the adsorption rate of Fe-REC was much higher than that of REC for simulated wastewater. For Cr(VI), the higher the pulp concentration, the higher adsorption rate of Fe-REC. When the pulp concentration rose to 70 g/L, the adsorption rate maintained stable gradually if it continued to increase. However, for Pb(II), only 40 g/L of pulp concentration was required for its excellent adsorption. By comparing Cr(VI) and Pb(II), the adsorption rate of Pb(II) was

far better than that of Cr(VI), which could attribute to the larger ionic volume of $Cr_2O_7^{2-}$ than that of Pb^{2+}, not conducive to accommodate pollutants by the interlayer of rectorite and causing the lower adsorption rate finally.

The effect of adsorption time was presented in Figure 4c. Although the adsorption rate of Cr(VI) with REC was raised by increasing time, the results were much worse than Fe-REC. When the time was defined at 30 min, the adsorption with Fe-REC was close to saturation, about 92.43%. For Pb(II), the adsorption rate had a slight downward trend after 50 min and remained steady between 30 to 50 min. Thus, 30 min was chosen as the optimum time for the pollutant adsorption.

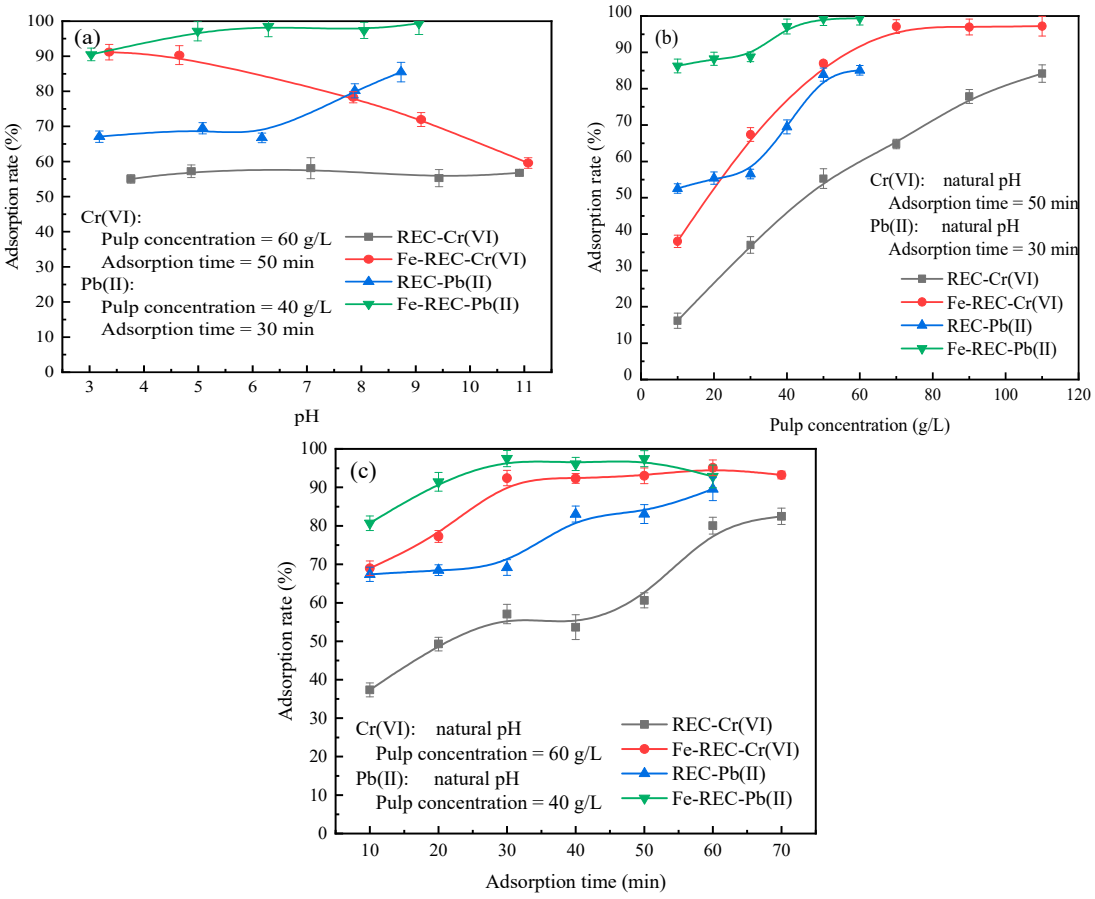

Figure 4. The effect of three different factors on Cr(VI) and Pb(II) adsorption with REC and Fe-REC. (**a**) pH; (**b**) pulp concentration and (**c**) adsorption time.

3.3. Zeta Potential Analysis

Figure 5 depicted the trend of rectorite zeta potential before and after its modification and adsorption with metal ions. Consistent with previous studies [26], the negative IEP (isoelectric point) value for the pure rectorite was –12.1 mV without any addition of reagents, indicating that zeta potential test was reliable. As shown in Figure 5, the potential on the REC surface decreased with the increasing pH and when the pH was 3.08, the potential was –0.25 mV, which was close to its PZC (point of zero charge). It could be concluded that the negative charge on the rectorite surface was almost neutralized. However, when the pulp was changed to more basic, the increasing high concentration of OH– made the potential more and more negative. When the REC was modified, namely Fe-REC, the zeta potentials exhibited a positive shift within the investigated pH range, which suggested that the positive Fe^{3+} ions were apparently adsorbed to balance a portion of negative charge on the mineral surface. Similar to the tendency of REC, zeta potential of Fe-REC was still dropped with pH and at the natural pH, the value of potential was –2.21 mV, increased by 9.89 mV than that of REC, illustrating

that the adsorption of Fe^{3+} on rectorite surface had brought greater changes in potential. According to Figure 5, there was an obvious negative shift after negative Cr(VI) ions was adsorbed by Fe-REC and the natural potential reduced to –33.2 mV from –2.21 mV. This explained Cr(VI) was indeed adsorbed on Fe-REC surface, resulting in the change of potential. When the positive Pb(II) ions were adsorbed on the Fe-REC surface, the zeta potential shifted positively, which illustrated some positive Pb(II) ions were adsorbed successfully, corresponding to its theoretical phenomena.

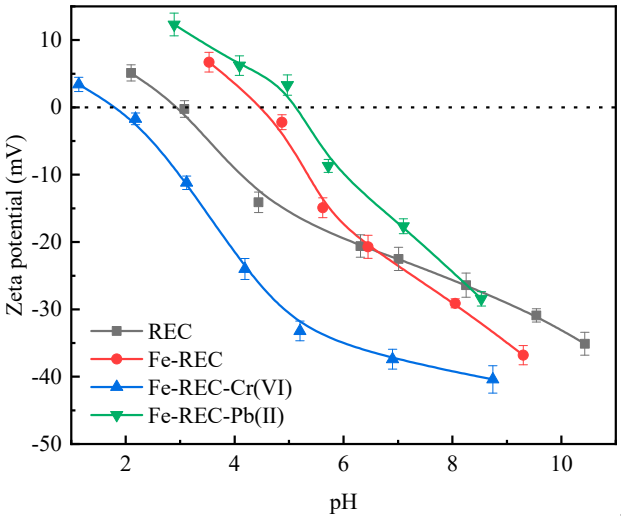

Figure 5. Zeta potential of rectorite before and after modification and adsorption.

3.4. XPS Analysis

Based on the chemical species on minerals surface and the distinctive binding energies of the inner electrons in each element, XPS analysis was performed to authenticate the interaction mechanism between the minerals and reagents [27]. The detailed values of atomic relative concentrations and binding energy of various components on the REC surface before and after some treatments are explained in this section.

Table 2 illustrated that comparing REC with Fe-REC, it was visible for Fe^{3+} to be adsorbed on the REC surface where the atomic relative concentration was about 1.38% causing the content of other mineral elements to decrease at the same time. This adsorption of Fe^{3+} perfectly coincided with the result of zeta potential in Figure 5, in which it was specifically because of the Fe^{3+} adsorption, making the potential on the REC surface shifted positively. Equally, 0.94% of Cr(VI) and 1.09% of Pb(II) occurred on the Fe-REC surface, respectively, after the treatment of adsorption by modified rectorite. Moreover, the adsorbed amount of Pb(II) was a little more than that of Cr(VI), agreeing with their adsorption tests in Section 3.3 where the adsorption capacity on Pb(II) was better than that of Cr(VI).

Table 2. The change of atomic relative concentration on the REC surface after its modification and adsorption.

Samples	Element (atomic %)						
	C 1s	O 1s	Al 2p	Si 2p	Fe 2p	Cr 2p	Pb 4f
REC	9.15	61.89	14.22	14.75	-	-	-
Fe-REC	11.16	61.75	12.45	13.26	1.38	-	-
Fe-REC-Cr(VI)	9.48	60.66	13.23	14.43	1.26	0.94	-
Fe-REC-Pb(II)	11.35	61.03	12.48	13.96	1.15	-	1.09

The binding energy and its shift on the REC surface treated by modification and adsorption were depicted in Table 3. The shifts in binding energy of the studied elements mainly revealed that the

reaction between Al species and Si species and their adsorption changed their chemical surrounding on REC surface. After the modification of REC, the shift of binding energy in O 1s was 0.37 eV, exceeding the measurement error range of 0.2 eV [28]. This shift meant the state of oxygen had undergone a chemical change during the adsorption of ferric chloride on the REC surface, indicating that the adsorption process of Fe^{3+} was chemisorption. For the shift between Fe-REC and Fe-REC-Cr(VI), –0.87eV of O 1s and –1.23eV of Fe 2p drew attention easily to manifest oxygen and iron elements changed chemically during the Cr(VI) adsorption. However, for Fe-REC-Pb(II), except oxygen and iron elements, the binding energy in the silicate mineral elements of Al and Si also changed greatly with 0.81 eV and 0.33 eV, respectively. These findings demonstrated that it was chemisorption that occurred during the adsorptions of Cr(VI) and Pb(II).

Table 3. Binding energy and its shift on the REC surface treated by modification and adsorption.

Samples	Binding Energy (eV)				
	C 1s	O 1s	Al 2p	Si 2p	Fe 2p
REC	284.76	531.52	74.8	102.99	-
Fe-REC	284.83	531.89	74.8	102.92	711.82
Shift values	0.07	0.37	0	−0.08	-
Fe-REC-Cr(VI)	284.82	531.02	74.82	103.07	710.59
Shift values	−0.01	−0.87	0.02	0.15	−1.23
Fe-REC-Pb(II)	284.81	530.74	75.61	103.25	710.04
Shift values	−0.02	−1.15	0.81	0.33	−1.78

Figure 6 showed XPS survey spectra of rectorite after modification and adsorption. From this figure, the emergence of Na and Ca elements was mainly due to interlayer cations of Na+ and Ca^{2+} in the mica or montmorillonite unit layer [14]. When the REC was modified by Fe^{3+}, significant characteristic peaks of Fe 2p appeared in XPS survey spectra, reflecting that the modifier Fe^{3+} had a strong adsorption on the surface of REC. As a comparison, we could not detect any weak peaks of Cr(VI) and Pb(II) appeared on the Fe-REC surface after their adsorption. This may result from only a trace of chromium and lead elements adsorbed on Fe-REC surface was covered up by miscellaneous peaks easily owing to 1% detection accuracy of XPS. However, the adsorption of Cr(VI) and Pb(II) was demonstrated in Tables 2 and 3.

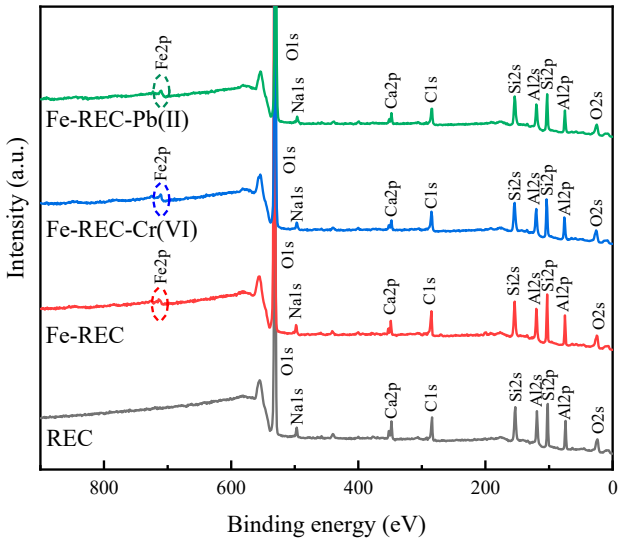

Figure 6. XPS survey spectra of rectorite before after modification and adsorption.

The high-resolution XPS spectra of Fe 2p in modified rectorite were shown in Figure 7 was reliable on account of better fitting results between raw intensity and peak sum. The main Fe 2p doublets peak

of Fe 2p3/2 and Fe 2p1/2 appeared at 710.12 eV and 723.94 eV, respectively. The peaks at 714.85 eV and 730.49 eV were attributed to the satellite of Fe 2p3/2 and Fe 2p1/2. These main peaks of Fe 2p were assigned to the oxidation state of Fe(III) [29–31], which further demonstrated the formation of Fe–O, Fe–OH and Fe–OOH on the Fe-REC surface. This conclusion explained why the binding energy of oxygen element changed dramatically during the modification of REC in Table 3.

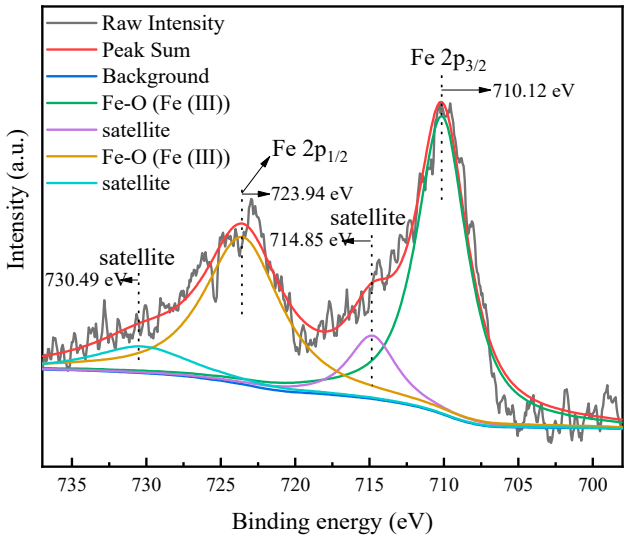

Figure 7. High-resolution XPS spectra of Fe 2p in modified rectorite.

3.5. Solution Chemistry Calculations

The hydroxyl complexation of Fe^{3+} in solution mainly exhibits in Table 4 [31]. According to the Equations (3)–(7) and (8)–(13), the species distribution of each component in the ferric chloride solution (0.1 mol/L) in different systems could be calculated and the result was shown in Figure 8.

Table 4. Equilibrium reaction and corresponding coefficients of different ions.

Ions	Reactions	Reaction Constants
Fe(III)	$Fe^{3+} + OH^- = [FeOH]^{2+}$	$\log \beta_1 = 11.81$ (14)
	$Fe^{3+} + 2OH^- = [FeOH]^{+}$	$\log \beta_2 = 22.3$ (15)
	$Fe^{3+} + 3OH^- = Fe(OH)_3(aq)$	$\log \beta_3 = 32.05$ (16)
	$Fe^{3+} + 4OH^- = Fe(OH)_4^-$	$\log \beta_4 = 34.3$ (17)
Cr(VI)	$CrO_4^{2-} + H^+ = HCrO_4^-$	$\log K_1 = -6.51$ (18)
	$HCrO_4^- + H^+ = H_2CrO_4$	$\log K_2 = 0.81$ (19)
	$2CrO_4^{2-} + 2H^+ = Cr_2O_7^{2-}$	$\log K_3 = -14.52$ (20)
Pb(II)	$Pb^{2+} + OH^- = [PbOH]^{+}$	$\log K_1 = 6.3$ (21)
	$Pb^{2+} + 2OH^- = Pb(OH)_2(aq)$	$\log K_2 = 10.9$ (22)
	$Pb^{2+} + 3OH^- = Pb(OH)_3^-$	$\log K_3 = 13.9$ (23)

Similar computing methods can also be applied in the species distribution of Cr(VI) and Pb(II), and both of their equilibrium reaction formulas and corresponding reaction coefficients were displayed in Table 4 [32,33]. Based on Table 4, the species distributions of 2.72×10^{-4} mol/L Cr(VI) and 0.91×10^{-4} mol/L Pb(II) were described in Figures 9 and 10. From Figure 8, the forms of Fe^{3+} in solution were mainly iron hydroxy complexes owing to 4–5 pH in the slurry solution, consisting of $FeOH^{2+}$, $Fe(OH)_2{}^+$ and $Fe(OH)_3$(aq). At the same time, the main species distribution of 2.72×10^{-4} mol/L Cr(VI) in Figure 9 in the same pH range were $HCrO_4{}^-$ and $CrO_4{}^{2-}$. Under this circumstance, the iron hydroxy

complex ($FeOH^{2+}$, $Fe(OH)_2{}^+$ and $Fe(OH)_3(aq)$) would react with $HCrO_4{}^-$ and $CrO_4{}^{2-}$ to promote the Cr(VI) adsorption on the Fe-REC surface according to the following equation [34]:

$$FeOH_2^+ + CrO_4^{2-} \rightleftharpoons FeCrO_4^- + H_2O \quad (24)$$

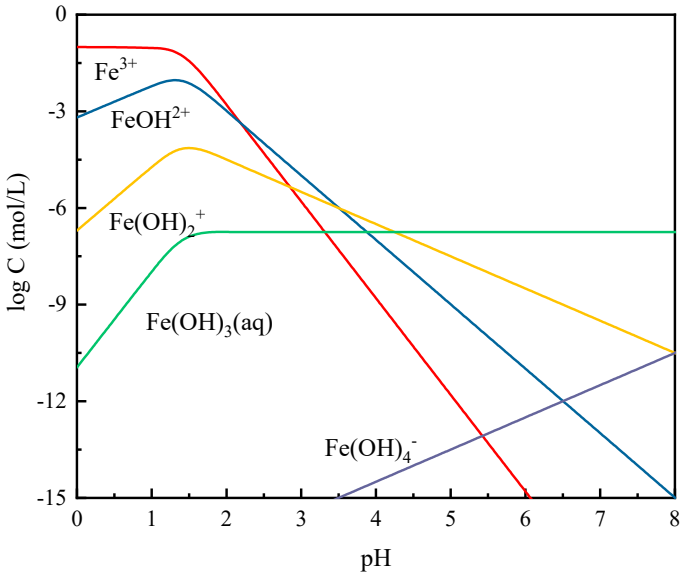

Figure 8. Species distribution diagram of 0.1 mol/L ferric chloride.

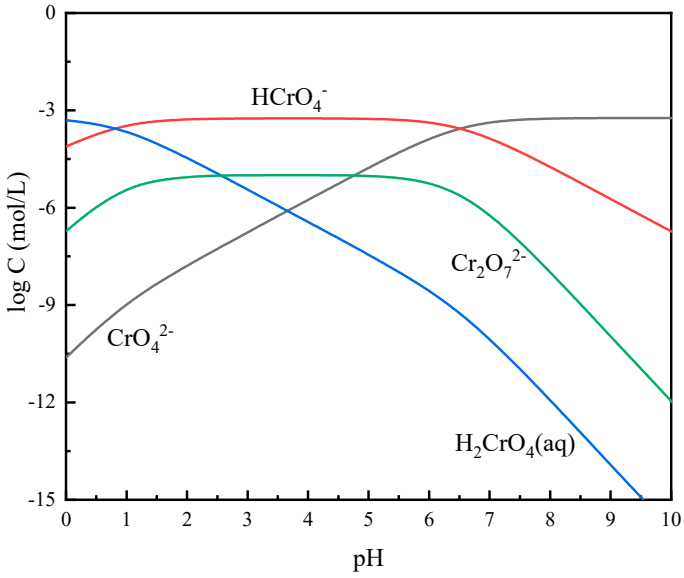

Figure 9. Species distribution diagram of 2.72×10^{-4} mol/L Cr(VI).

Therefore, this explained why the binding energy of Fe and Cr elements happened to change over 0.2 eV during the Cr(VI) adsorption in XPS analysis (shown in Table 3).

Illustrated by Figure 10, the species distribution of 0.91×10^{-4} mol/L lead ions solution were primarily Pb^{2+} and $PbOH^+$ for pH ranging from 4 to 5. Owing to the existence of –Al–OH and –Si–OH of silicate rectorite in the slurry, these groups would react with the main species of Pb(II) as below [35]:

$$SOH + PbOH^+ = SOPbOH + H^+ \quad (25)$$

$$SO^- + PbOH^+ = SOPbOH \quad (26)$$

where SOH represents –Al–OH and –Si–OH; SO^- denotes forms of SOH losing H^+.

As a result, the adsorption mechanism of Pb(II) on the Fe-REC surface was as followed. The solid–liquid interface induced the hydrolysis of Pb to generate the $PbOH^+$ colloid with a positive charge, which would interact with negatively charged aluminosilicate to ultimately improve the Pb(II) adsorption, accordant with the results in XPS analysis (Table 3) where the binding energy of aluminum and silicon elements varied greatly during the process of Pb(II) adsorption. In this scenario, the role of Fe^{3+} was to weaken interlayer bond force to enhance the Pb(II) adsorption.

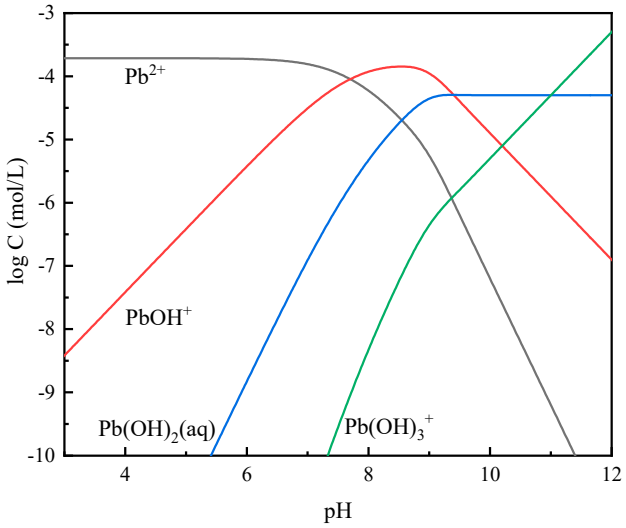

Figure 10. Species distribution diagram of 0.91×10^{-4} mol/L Pb(II).

3.6. Adsorption Isotherms

In aqueous solution, Langmuir and Freundlich models are usually used for the adsorption isotherms of heavy metal ions. What Langmuir isotherm assumes is the monolayer adsorption onto a uniform solid surface with no transmigration of adsorbate on the plane surface [36]. The isotherm is represented by [37]

$$\frac{C_e}{q_e} = \frac{C_e}{q_m} + \frac{1}{K_L q_m} \tag{27}$$

where C_e is equilibrium concentration, mg/L; q_e is equilibrium adsorption capacity, mg/g; q_m is maximum adsorption capacity, mg/g; K_L is adsorption energy, L/g; The linear plot of specific adsorption (C_e/q_e) against the equilibrium concentration (C_e) shows that the adsorption obeys the Langmuir model. Values of q_m and the constant K_L can be acquired from the slope and interception of the plot, respectively.

Freundlich is applied as an empirical model in which the isotherm is represented by [38]

$$\log q_e = logK_F + \frac{1}{n} logC_e \tag{28}$$

where adsorption capacity K_F and adsorption intensity n are parameters that depend on the adsorbate and adsorbent, determined from the plot of $\log q_e$ versus $\log C_e$.

On the basis of the above Equations (27)–(28), Langmuir and Freundlich isotherms for Cr(VI) and Pb(II) adsorption are provided in Figures 11 and 12, respectively. In addition, their constants and correlation coefficients (R^2) are presented in Table 5. When it comes to Cr(VI) adsorption, the result of Freundlich isotherm (R^2 = 0.9908) was superior to that of Langmuir (R^2 = 0.9618), indicating that the isothermal adsorption of Cr(VI) was more compatible with Freundlich model. There is the reference to prove that if the n value in Freundlich model ranges from 1 to 10, the adsorption process will be effective [39]. Thus, the Cr(VI) adsorption process on the Fe-REC surface happened effectively

(n = 3.2146). For Pb(II) adsorption, it was more consistent with Langmuir isotherm (R^2 = 0.9959) by comparing two kinds of models and the maximum adsorption capacity of Pb(II) was 1.3509 mg/g.

Table 5. Isotherm parameters for Cr(VI) and Pb(II) adsorption by Fe-REC.

Metals Ions	Langmuir			Freundlich		
	q_m (mg/g)	K_L (L/g)	R^2	K_F (mg/g)	n(g/L)	R^2
Cr(VI)	1.7128	2.8927	0.9618	1.1019	3.2146	0.9908
Pb(II)	1.3509	0.8914	0.9959	0.6330	3.9568	0.9763

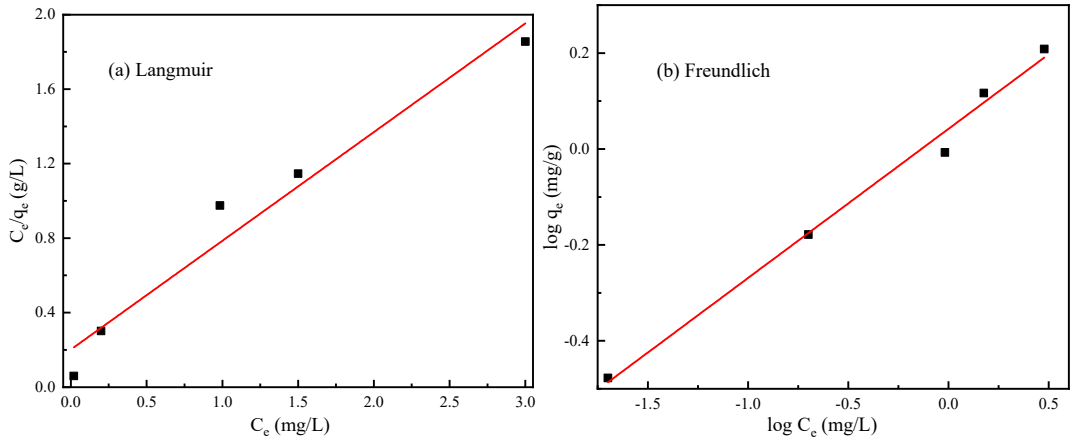

Figure 11. Langmuir (**a**) and Freundlich (**b**) isotherms for Cr(VI) adsorption by Fe-REC.

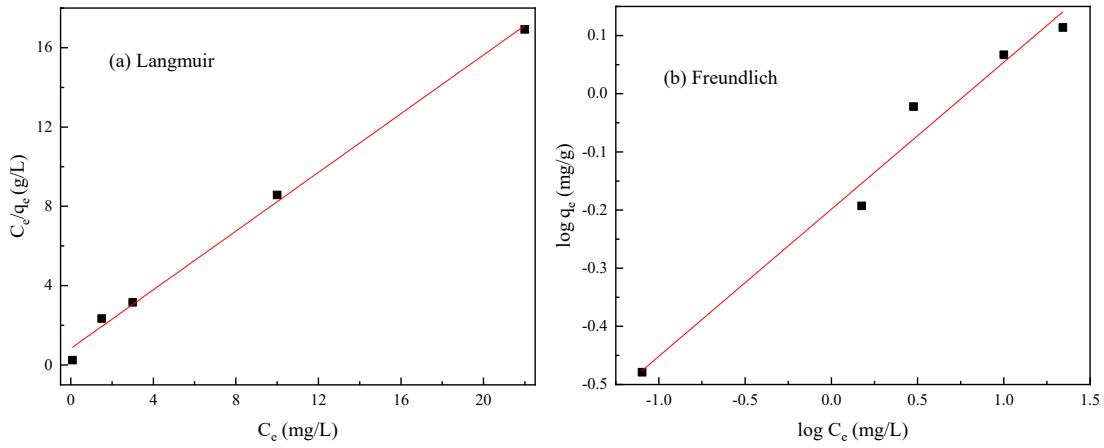

Figure 12. Langmuir (**a**) and Freundlich (**b**) isotherms for Pb(II) adsorption by Fe-REC.

The model of modification and adsorption was shown in Figure 13 where some cations (Na^+, K^+ and Ca^{2+}) were distributed on the surface of layered rectorite. When ferric chloride hexahydrate was added into the pulp, Fe^{3+} would be adsorbed on the REC surface as its oxidation state (Fe–O), which can be proved by the significant characteristic peaks of Fe 2p appeared in XPS survey spectra. Since the interlayer bond force of rectorite was weakened, more produced vacancy promoted the Pb(II) adsorption significantly. In addition, the reactions between $PbOH^+$ and –AlOH or –SiOH also contributed to its adsorption capacity tremendously. The Cr(VI) adsorption process resulted from its main species in aqueous solution reacted with the Fe–O ($FeOH^{2+}$, $Fe(OH)_2{}^+$ and $Fe(OH)_3$(aq)) on the REC surface. Therefore, rectorite modification with Fe(III) can improve the removal of heavy metal ions distinctly.

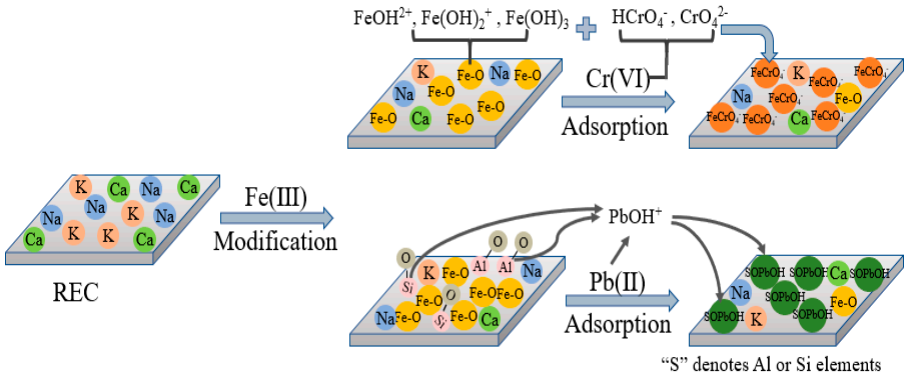

Figure 13. Schematic diagram of REC modification and Cr(VI) and Pb(II) adsorption.

4. Conclusions

This investigation showed that the novel modifier Fe^{3+} chemisorption on the REC surface improved its adsorption capacity for Cr(VI) and Pb(II). For Fe-REC, the potential exhibited a positive shift within the studied pH range. In the XPS survey spectra, significant characteristic peaks of Fe 2p appeared, which was the oxidation state of Fe(III) (Fe–O, Fe–OH, Fe–OOH) formed on the Fe-REC surface.

The Cr(VI) adsorption mechanism was mainly due to the reaction between the iron hydroxy complex of modifier ($FeOH^{2+}$, $Fe(OH)_2{}^+$ and $Fe(OH)_3$(aq)) and the major components of hexavalent chromium solution ($HCrO_4{}^-$ and $CrO_4{}^{2-}$) to promote its adsorption behavior. From zeta potential results, there was an obvious negative shift after Cr(VI) ions was adsorbed by Fe-REC and the natural potential reduced to –33.2 mV from –2.21 mV. In XPS analysis, the binding energy of O 1s and Fe 2p changed a lot. This resulted in chemical changes of oxygen and iron elements during its adsorption. This adsorption process was consisted with Freundlich isotherm.

While for Pb(II), there was $PbOH^+$ colloid appeared due to the lead ions hydrolysis induced by the solid liquid interface. It would react with the groups of –Al–OH and –Si–OH in silicate REC slurry, profiting Pb(II) adsorption. Zeta potential shifted positively after Pb(II) adsorption, corresponding to its theoretical phenomena. In XPS analysis, binding energy in silicate elements of Al and Si changed greatly (0.81 eV and 0.33 eV) to explain its adsorption mechanism. The Pb(II) adsorption was more accordant with Langmuir isotherm and its maximum adsorption capacity was 1.3509 mg/g.

Author Contributions: Conceptualization, H.J. and X.L.; methodology, H.J. and Y.G.; formal analysis, H.J., X.L.; investigation, Y.G.; writing—original draft preparation, Y.G.; writing—review and editing, S.A.K., G.X. and W.H. All authors have read and agreed to the published version of the manuscript.

Funding: Authors of this paper proudly acknowledged the financial supports from National Natural Science Foundation of China (Grant Nos. 51634009 and 51374247) and the National Key Scientific Research Project (2018YFC1901601 and 2018YFC1901602).

Conflicts of Interest: The authors declare no conflict of interest.

References

1. Chen, Z.; Li, Y.; Guo, M.; Xu, F.; Wang, P.; Du, Y.; Na, P. One-pot synthesis of Mn-doped TiO_2 grown on graphene and the mechanism for removal of Cr(VI) and Cr(III). *J. Hazard. Mater.* **2016**, *310*, 188–198. [CrossRef]
2. Song, W.; Shi, T.; Yang, D.; Ye, J.; Zhou, Y.; Feng, Y. Pretreatment effects on the sorption of Cr(VI) onto surfactant-modified zeolite: Mechanism analysis. *J. Environ. Manag.* **2015**, *162*, 96–101. [CrossRef] [PubMed]
3. Nam, A.; Choi, U.S.; Yun, S.T.; Choi, J.W.; Park, J.A.; Lee, S.H. Evaluation of amine-functionalized acrylic ion exchange fiber for chromium (VI) removal using flow-through experiments modeling and real wastewater. *J. Ind. Eng. Chem.* **2018**, *66*, 187–195. [CrossRef]

4. Gupta, V.K.; Gupta, M.; Sharma, S. Process development for the removal of lead and chromium from aqueous solutions using red mud—An aluminium industry waste. *Water Res.* **2001**, *35*, 1125–1134. [CrossRef]
5. Sekhar, K.C.; Kamala, C.T.; Chary, N.S.; Sastry, A.R.K.; Rao, T.N.; Vairamani, M. Removal of lead from aqueous solutions using an immobilized biomaterial derived from a plant biomass. *J. Hazard. Mater.* **2004**, *108*, 111–117.
6. Taka, A.L.; Fosso-Kankeu, E.; Pillay, K.; Mbianda, X.Y. Removal of cobalt and lead ions from wastewater samples using an insoluble nanosponge biopolymer composite: Adsorption isotherm, kinetic, thermodynamic, and regeneration studies. *Environ. Sci. Pollut. Res.* **2018**, *25*, 21752–21767. [CrossRef] [PubMed]
7. Fu, F.; Wang, Q. Removal of heavy metal ions from wastewaters: A review. *J. Environ. Manag.* **2011**, *92*, 407–418. [CrossRef] [PubMed]
8. Wang, T.; Jin, X.; Chen, Z.; Megharaj, M.; Naidu, R. Simultaneous removal of Pb(II) and Cr(III) by magnetite nanoparticles using various synthesis conditions. *J. Ind. Eng. Chem.* **2014**, *20*, 3543–3549. [CrossRef]
9. Eskandari, E.; Kosari, M.; Davood Abadi Farahani, M.H.; Khiavi, N.D.; Saeedikhani, M.; Katal, R.; Zarinejad, M. A review on polyaniline-based materials applications in heavy metals removal and catalytic processes. *Sep. Purif. Technol.* **2020**, *231*, 115901. [CrossRef]
10. Izidoro, J.D.C.; Fungaro, D.A.; Abbott, J.E.; Wang, S. Synthesis of zeolites X and A from fly ashes for cadmium and zinc removal from aqueous solutions in single and binary ion systems. *Fuel* **2013**, *103*, 827–834. [CrossRef]
11. Guan, B.; Ni, W.; Wu, Z.; Lai, Y. Removal of Mn(II) and Zn(II) ions from flue gas desulfurization wastewater with water-soluble chitosan. *Sep. Purif. Technol.* **2009**, *65*, 269–274. [CrossRef]
12. Shin, K.Y.; Hong, J.Y.; Jang, J. Heavy metal ion adsorption behavior in nitrogen-doped magnetic carbon nanoparticles: Isotherms and kinetic study. *J. Hazard. Mater.* **2011**, *190*, 36–44. [CrossRef] [PubMed]
13. Huang, Y.; Zeng, X.; Guo, L.; Lan, J.; Zhang, L.; Cao, D. Heavy metal ion removal of wastewater by zeolite-imidazolate frameworks. *Sep. Purif. Technol.* **2018**, *194*, 462–469. [CrossRef]
14. Huang, Y.; Ma, X.; Liang, G.; Yan, Y.; Wang, S. Adsorption behavior of Cr(VI) on organic-modified rectorite. *Chem. Eng. J.* **2008**, *138*, 187–193. [CrossRef]
15. Liu, Z.; Chen, L.; Dong, Y.; Zhang, Z. Impact of environmental conditions on the sorption behavior of Co(II) on Na-rectorite studied by batch experiments. *Chem. Eng. J.* **2011**, *289*, 851–859. [CrossRef]
16. Huang, J.; Ming, Y.A.; Du, Y.; Wang, Y.; Wang, C.E. Study on the effect of the three-dimensional electrode in degradation of methylene blue by lithium modified rectorite. *J. Anal. Methods Chem.* **2016**, *2016*, 1–6. [CrossRef]
17. Mei, H.; Yu, S.; Tan, X.; Wang, S.; Chen, C.; Li, J. Evaluation of the influence of environmental conditions on the removal of Pb(II) from wastewater by ca-rectorite. *Sep. Sci. Technol.* **2015**, *50*, 2257–2266. [CrossRef]
18. Tu, H.; Huang, M.; Yi, Y.; Li, Z.; Zhan, Y.; Chen, J.; Wu, Y.; Shi, X.; Deng, H.; Du, Y. Chitosan-rectorite nanospheres immobilized on polystyrene fibrous mats via alternate electrospinning /electrospraying techniques for copper ions adsorption. *Appl. Surf. Sci.* **2017**, *426*, 545–553. [CrossRef]
19. Zeng, L.; Chen, Y.; Zhang, Q.; Guo, X.; Peng, Y.; Xiao, H.; Chen, X.; Luo, J. Adsorption of Cd(II), Cu(II) and Ni(II) ions by cross-linking chitosan/rectorite nano-hybrid composite microspheres. *Carbohydr. Polym.* **2015**, *130*, 333–343. [CrossRef]
20. Xie, M.; Zeng, L.; Zhang, Q.; Yuan, K.; Xiao, H.; Peng, Y.; Chen, X.; Luo, J. Synthesis and adsorption behavior of magnetic microspheres based on chitosan/organic rectorite for low-concentration heavy metal removal. *J. Alloy. Compd.* **2015**, *647*, 892–905. [CrossRef]
21. Hong, H.; Jiang, W.T.; Zhang, X.; Tie, L.; Li, Z. Adsorption of Cr(VI) on STAC-modified rectorite. *Appl. Clay Sci.* **2008**, *42*, 292–299. [CrossRef]
22. Ying, Z.; Shao, Z.; Chen, C.; Hu, J.; Chen, H. Effect of environmental conditions on the adsorption behavior of Sr(II) by Na-rectorite. *Appl. Clay Sci.* **2014**, *87*, 1–6.
23. Xu, Y.; Chen, J.; Chen, R.; Yu, P.; Guo, S.; Wang, X. Adsorption and reduction of chromium(VI) from aqueous solution using polypyrrole/calcium rectorite composite adsorbent. *Water Res.* **2019**, *160*, 148–157. [CrossRef]
24. Tu, H.; Yu, Y.; Chen, J.; Shi, X.; Zhou, J.; Deng, H.; Du, Y. Highly cost-effective and high-strength hydrogels as dye adsorbents from natural polymers: Chitosan and cellulose. *Polym. Chem.* **2017**, *8*, 2913–2921. [CrossRef]
25. Wang, D.; Hu, Y. *Flotation Solution Chemistry*; Hunan Science and Technology Press: Changsha, China, 1988; pp. 132–138.

26. Wang, X.; Bo, L.; Ren, J.; Liu, C.; Wang, X.; Wu, J.; Sun, R. Preparation and characterization of new quaternized carboxymethyl chitosan/rectorite nanocomposite. *Compos. Sci. Technol.* **2010**, *70*, 1161–1167. [CrossRef]
27. Tian, J.; Xu, L.; Sun, W.; Zeng, X.; Fang, S.; Han, H.; Hong, K.; Hu, Y. Use of $Al_2(SO_4)_3$ and acidified water glass as mixture depressants in flotation separation of fluorite from calcite and celestite. *Miner. Eng.* **2019**, *137*, 160–170. [CrossRef]
28. Dong, L.; Jiao, F.; Qin, W.; Zhu, H.; Jia, W. Selective depressive effect of sodium fluorosilicate on calcite during scheelite flotation. *Miner. Eng.* **2019**, *131*, 262–271. [CrossRef]
29. Tian, M.; Liu, R.; Gao, Z.; Pan, C.; Han, H.; Li, W.; Zhang, C.; Wei, S.; Hu, Y. Activation mechanism of Fe (III) ions in cassiterite flotation with benzohydroxamic acid collector. *Miner. Eng.* **2018**, *119*, 31–37. [CrossRef]
30. Peng, J.; Moszner, F.; Rechmann, J.; Vogel, D.; Palm, M.; Rohwerder, M. Influence of Al content and pre-oxidation on the aqueous corrosion resistance of binary Fe-Al alloys in sulphuric acid. *Corros. Sci.* **2019**, *149*, 123–132. [CrossRef]
31. Wei, Q.; Dong, L.; Jiao, F.; Qin, W. Use of citric acid and Fe(III) mixture as depressant in calcite flotation. *Colloids Surf. A Physicochem. Eng. Asp.* **2019**, *578*, 123579. [CrossRef]
32. Weerasooriya, R.; Tobschall, H.J. Mechanistic modeling of chromate adsorption onto goethite. *Colloids Surf. A Physicochem. Eng. Asp.* **2000**, *162*, 167–175. [CrossRef]
33. Senanayake, G. A review of effects of silver, lead, sulfide and carbonaceous matter on gold cyanidation and mechanistic interpretation. *Hydrometallurgy* **2008**, *90*, 46–73. [CrossRef]
34. Deng, Y.; Stjernström, M.; Banwart, S. Accumulation and remobilization of aqueous chromium(VI) at iron oxide surfaces: Application of a thin-film continuous flow-through reactor. *J. Contam. Hydrol.* **1996**, *21*, 141–151. [CrossRef]
35. Bradbury, M.H.; Baeyens, B. Modelling the sorption of Mn(II), Co(II), Ni(II), Zn(II), Cd(II), Eu(III), Am(III), Sn(IV), Th(IV), Np(V) and U(VI) on montmorillonite: Linear free energy relationships and estimates of surface binding constants for some selected heavy metals and actinides. *Geochim. Cosmochim. Acta* **2005**, *69*, 875–892. [CrossRef]
36. Hameed, B.H.; Din, A.T.M.; Ahmad, A.L. Adsorption of methylene blue onto bamboo-based activated carbon: Kinetics and equilibrium studies. *J. Hazard. Mater.* **2007**, *141*, 819–825. [CrossRef]
37. Laatikainen, M.; Lindström, M. Determination of adsorption isotherms with quartz crystal microbalance in liquid phase. *J. Colloid Interface Sci.* **1988**, *125*, 610–614. [CrossRef]
38. Demirbas, A.; Sari, A.; Isildak, O. Adsorption thermodynamics of stearic acid onto bentonite. *J. Hazard. Mater.* **2006**, *135*, 226–231. [CrossRef]
39. Tahir, S.S.; Naseem, R. Removal of Cr(III) from tannery wastewater by adsorption onto bentonite clay. *Sep. Purif. Technol.* **2007**, *53*, 312–321. [CrossRef]